Dinuclear Diazene Iron and Ruthenium Complexes as Models for Studying Nitrogenase Activity**

Markus Reiher,*[a] Oliver Salomon,[a] Dieter Sellmann,[b] and Bernd Artur Hess[a]

Abstract: The strength of hydrogen bonds has been investigated in various dinuclear diazene Fe^{II}, Fe^{III}, and Ru^{II} complexes by use of the recently developed shared-electron number approach. Hydrogen bonding in these compounds plays an essential role in view of designing a model system for nitrogenase activity. The general conclusions for iron–sulfur complexes are: hydrogen bonds can stabilize diazene by at least 20 % of the total coordination energy; the strength of the hydrogen bonds can be directly controlled through the hydrogen–sulfur bond length; reducing Fe^{III} centers to Fe^{II} can double the hydrogen bond energy.

Keywords: density functional calculations · diazene complexes · hydrogen bonds · nitrogen fixation · iron/ruthenium sulfur complexes

Introduction

Biological N_2 fixation, the reduction of N_2 to NH_3 catalyzed by FeMo, FeV, or FeFe nitrogenases, is one of the fundamental synthetic processes of nature.[2–4] In spite of intensive efforts over the last decades, its molecular mechanism is poorly understood, in particular because the pivotal chemical question has remained unanswered: how do nitrogenases manage to activate and convert the inert N_2 molecule under ambient conditions at mild redox potentials? All abiological N_2-reducing systems either need drastic conditions, see for example, the Haber–Bosch process, or abiologically strong reductants such as alkaline metals.[5, 6] In addition, these strong-reductant-type N_2-reducing systems, which include a few metal dinitrogen complexes, do not function catalytically.[7, 8] Hence, all mechanistic proposals for biological N_2 fixation that are based on such systems are left with the problem of how to explain how nitrogenases enable catalytic N_2 reduction at mild biological reduction potentials.[9, 10] These reduction potentials probably represent the biggest challenge in the search for synthetic competitive catalysts that function with nitrogenase-like activity. Thermodynamics states that the redox potential for the reaction according to Equation (1) is $E = -280$ mV at pH 7,[11–13] and biological redox systems rarely operate at potentials lower than $E = -700$ mV.[11–16]

$$N_2 + 6H^+ + 6e^- \rightarrow 2NH_3 \qquad E^\circ = -280\ \text{mV, pH 7} \qquad (1)$$

Such conditions can potentially be met by systems that operate according to the "open-side" model for the cofactor function of FeMo, FeV, or FeFe nitrogenases.[14–16] The "open-side" model suggests that the FeMo cofactor (FeMoco) exhibits different structures in the resting state (depicted in Scheme 1) and in the turn-over state. It proposes that one Fe-S-Fe bridge is cleaved in the turn-over state and that vicinal

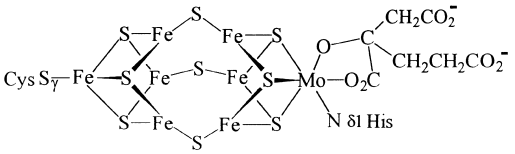

Scheme 1. Resting state of the FeMo cofactor of nitrogenase.

water molecules and donor atoms of the two amino acids Glnα191 and Hisα195, which are essential for the activity of nitrogenase, are added to give two unique five-coordinate Fe^{II} centers with Brönsted basic sulfur donors (Scheme 2). These Fe centers bind N_2, which is converted by three consecutive $2H^+/2e^-$ transfer steps into N_2H_2, N_2H_4, and finally to two NH_3. Scheme 3 schematically shows the first $2H^+/2e^-$ reduction step, which is probably the most difficult step for thermodynamic and kinetic reasons. The primary protonation of the Brönsted-basic sulfur donors in A ultimately enables

[a] Dr. M. Reiher, O. Salomon, Prof. Dr. B. A. Hess
Lehrstuhl für Theoretische Chemie
Universität Erlangen-Nürnberg
Egerlandstrasse 3, 91058 Erlangen (Germany)
Fax: (+49) 9131-85-2773
E-mail: markus.reiher@chemie.uni-erlangen.de
hess@chemie.uni-erlangen.de

[b] Prof. Dr. D. Sellmann
Lehrstuhl für Anorganische und Allgemeine Chemie
Universität Erlangen-Nürnberg
Egerlandstrasse 1, 91058 Erlangen (Germany)

[**] Stabilization of Diazene in Iron Sulfur Complexes Relevant for Nitrogenase Activity, Part II; for Part I see: Ref. [1]

Supporting information for this article is available on the WWW under http://wiley-vch.de/home/chemistry/ or from the author.

  0947-6539/01/0723-5195 $ 17.50+.50/0

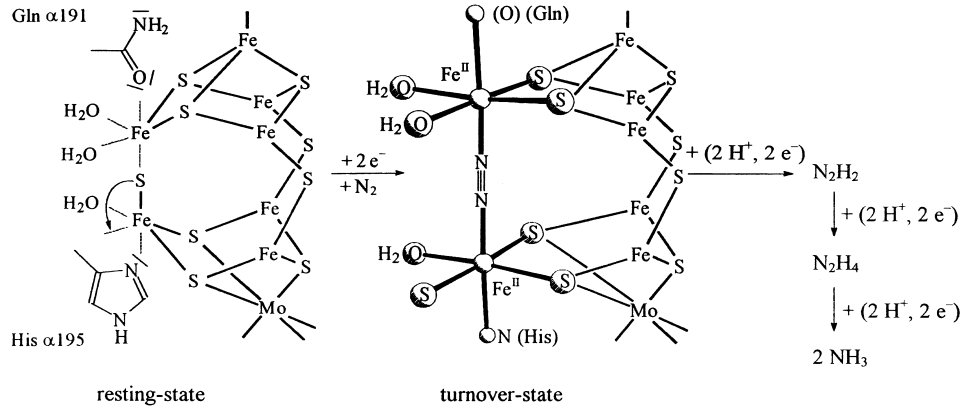

Scheme 2. Open-side model for the turn-over state of FeMoco.

the subsequent two-electron transfer to the N_2 ligand and the formation of the N_2H_2 species D.

The "open-side" model and the Scheme 3 take account of a large number of biological, biochemical, and chemical results:

1) All nitrogenase substrates are reduced by transfer steps that are multiples of $2H^+/2e^-$.[17]
2) N_2H_2, which is extremely unstable in the free state, is highly stabilized by coordination to iron–sulfur complex fragments.[18–21]
3) Primary protonation of Brönsted-basic sulfur donors anodically shifts the redox potentials of iron–sulfur ligand complexes such that they become reducible at potentials of about -500 mV.[22]
4) Only iron oxidation states accessible in aqueous phase are involved.
5) N_2H_2 complexes modeling the nitrogenase-catalyzed "N_2-dependent HD formation from D_2/H^+ exchange" support diazene as the key intermediate of N_2 fixation.[16, 23–25]

Scheme 3 stresses a close coupling of proton- and electron-transfer steps. This has also been pointed out by Collman et al. for the redox reactions of dinuclear porphyrinato–ruthenium complexes that bind N_2, N_2H_2, N_2H_4, and NH_3.[26] The scheme further emphasizes the importance of hydrogen bridges for the $N_2 \rightarrow N_2H_2$ conversion. N-H···S hydrogen bridges in species B favor the primary protonation of the neutral [μ-$N_2\{FeS_2\}_2$] species A, and bifurcated N-H···$(S)_2$ bridges in D favor the stabilization of N_2H_2 that results from the $2e^-$ transfer. On the basis of experimental data, it has been estimated that the bifurcated N-H···$(S)_2$ bridges may contribute up to 70 kJ mol^{-1} to the total stabilization energy of coordinated N_2H_2; this facilitates the first and most difficult $N_2 \rightarrow N_2H_2$ reduction step.[15, 18] While the steps A → B → C of Scheme 3 remain as yet hypothetical, the reversible step C ⇌ D has been established experimentally for a number of iron and analogous ruthenium complexes exhibiting [μ-$N_2H_2\{M(S)_2\}_2$] core structures with sulfur thiolate donors.[18–21, 27] Compounds with the structural features of species A or B are unknown. Thus, a complete characterization of all four species A to D by theoretical methods and, in particular, an elucidation of their relative energies can be anticipated to validate the viability of the "open-side" model for the nitrogenase cofactor function. Ultimately, insight into the molecular mechanism of a biological process could be gained that might be inaccessible by experimental methods.

A cornerstone in such investigations is the elucidation of the hydrogen bond energies in species B to D. For example, it can be hypothesized that strong hydrogen bonds destabilize B and simultaneously stabilize C or D. The whole process A → D might be further driven by the structural change when the linear [μ-$N_2\{M\}_2$] entity in A or B transforms into the bent [μ-$N_2H_2\{M\}_2$] entity in C or D.

The evaluation of the hydrogen bond energies in species such as B, C, or D is the objective of this work. In a previous work[1] (referred to as Part I in the following) a new approach, the shared-electron number (SEN) method, has been developed for the evaluation of hydrogen bonds in nondecomposable compounds, that is, in compounds which cannot be decomposed into two parts such that the decomposition energy can be solely attributed to the broken hydrogen bond. In Part I, we applied the SEN approach to mononuclear Fe^{II}–S model complexes. Here, this work is extended to their dinuclear analogues given in Scheme 4, which are experimentally accessible and have been characterized in great detail.[15, 18–21, 28] In view of the protonation and reduction process it is instructive to compare results for Fe^{II} compounds with the corresponding data for the positively charged Fe^{III} analogues. Iron and ruthenium complexes with two metal centers as shown in Scheme 4 were investigated. While the iron complexes model particular features of the FeMo-cofactor in nitrogenase, the ruthenium analogues are analyzed because of their synthetic importance: sometimes they are more stable than their iron analogues and represent useful compounds for testing synthetic strategies that can later be transferred onto their less-stable Fe^{II} homologues.

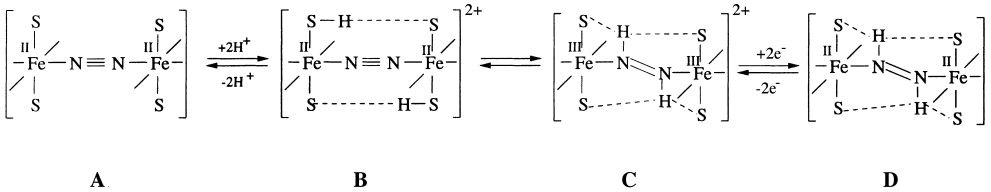

Scheme 3. Schematic representation of $2H^+/2e^-$ protonation-reduction of a dinitrogen complex.

0947-6539/01/0723-5196 $ 17.50+.50/0 *Chem. Eur. J.* **2001**, *7*, No. 23

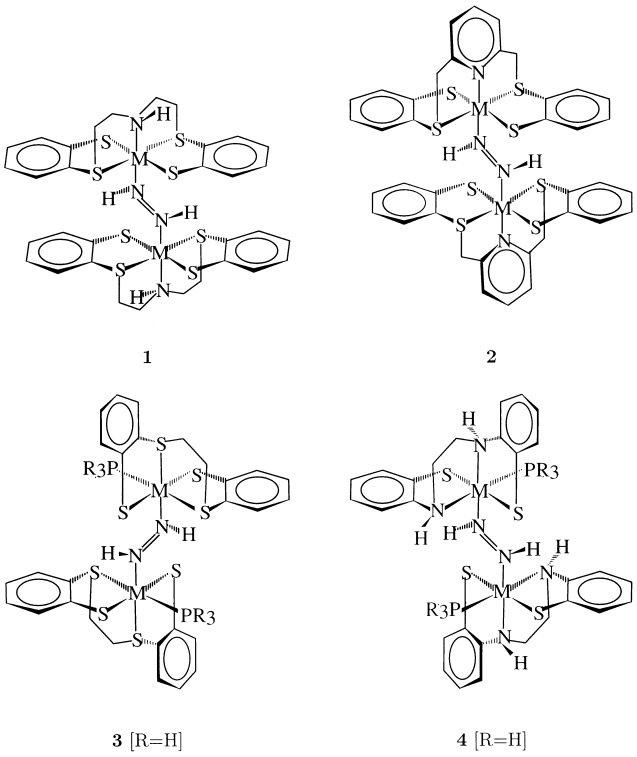

Scheme 4. Lewis structures of the dinuclear diazene compounds with M = Fe^{II}, Fe^{III}, Ru^{II} under study.

The work is organized as follows: The structural details of the four different types of chelate complexes depicted in Scheme 4 are described in the following section. Then, the SEN method is used to estimate the intramolecular hydrogen bond energies. A detailed description of the quantum chemical methodology employed is given under Computational Methods.

Optimized structures of the model complexes: The dinuclear metal–diazene complexes under study were chosen by following the lines of synthetic work on such compounds closely.[15, 18–21, 28] Their schematic structures are shown in Scheme 4. It is to be noted that such diazene complexes can form different diastereomers. We have studied only the representatives depicted in Scheme 4.

All dinuclear complexes contain a *trans*-diazene bridging two enantiomeric mononuclear fragments arranged to give C_1 symmetry for the dinuclear compound. The optimized structures of all complexes are shown in Figure 1. In order to analyze the reliability of the bond lengths and angles obtained from calculations with the functionals BP86/RI and B3LYP, we compared the calculated structure parameters with those obtained from X-ray diffraction experiments, which are available for the Fe^{II} complexes **1** and **3**. Tables 1 and 2 give selected bond lengths and angles for these complexes obtained with the TZVP basis set in connection with the BP86/RI and B3LYP functionals and compare these to the experimental values. In most cases, bond angles calculated with BP86/RI and B3LYP are almost identical and differ by less than 2° from each other. Apart from the α_{FeNH} angle in Fe^{II}–**1**, all angles are in very good agreement with the angles found experimentally. As far as bond lengths are concerned, the BP86/RI/TZVP lengths are closer to experiment than those obtained with the B3LYP functional. The BP86/RI bond lengths differ by about 2–3 pm from the experimental values, while the B3LYP lengths are always up to 7 pm larger than the experimental ones. The differences of the calculated and measured S–H and N–H lengths deviate from these general results; this is due to the fact that they are experimentally as well as quantum chemically difficult to determine since they bear only little electronic density and the potential energy well of the hydrogen bond is rather shallow.

In Figure 2, H···S lengths d_{HS} and H-N···S angles α_{HNS} for all complexes under consideration are defined. Their particular values are given in Tables 3 and 4. Since other structural parameters are of little importance with respect to hydrogen bonding, we refer the reader for further structure data to the cartesian coordinates given in the Supporting Information.

The *trans*-diazene moiety is always oriented parallel to the thiolate sulfur atoms of the chelate ligands. Complexes **1** and **2** as well as **3** and **4** are similar with respect to the arrangement of benzene rings. The arrangement of two benzene rings within one mononuclear half of these complexes determines the steric direction of the sulfur lone pairs (as discussed extensively in Part I) and is consequently a means of controlling hydrogen bonding.

The structures of complexes **1**–**4** in their dicationic form are very similar to those of their uncharged form. This can be traced back to the rigid chelate ligands. Therefore, reducing the Fe^{III} complexes to Fe^{II} complexes does not result in essential changes of the overall structures. However, large changes can be found for the H···S lengths; this is important for the corresponding change in hydrogen bond energies. The change of these H···S lengths by up to 20 pm is brought about by small changes of the angle of the *trans*-diazene plane relative to the plane defined by the two metal centers and four thiolate sulfurs, and by an increase in M–S bond length.

Comparison of the Fe^{II} and Ru^{II} complexes shows that the mononuclear fragments are again almost unchanged, while the M–N bond length is increased by about 15 pm on going from Fe^{II} to Ru^{II}.

Hydrogen bond energies:

Individual hydrogen bond energies: We evaluated the hydrogen bond energies according to the SEN method presented in Part I. The hydrogen bond energies $E^{SEN}_{(HS)_i}$ for each hydrogen-sulfur bridge $(HS)_i$ are given in Tables 5 and 6. According to the Lewis structures in Scheme 4, every dinuclear complex may contain at most four hydrogen bonds of which two are always equal in the case of C_1 symmetry. We distinguished two pairs of long and short hydrogen bonds. Hydrogen bond energies for the long hydrogen bridges, which are larger than about 5 kJ mol^{-1}, were only observed for **1** and **2** with Fe^{II} as central metal atoms. All other *long* hydrogen bonds were negligibly small, that is, weaker than approximately 2 kJ mol^{-1}. Only two short hydrogen bridges remained in these cases. Bifurcated hydrogen bridges are only present in Fe^{II}–**1** and Fe^{II}–**2**.

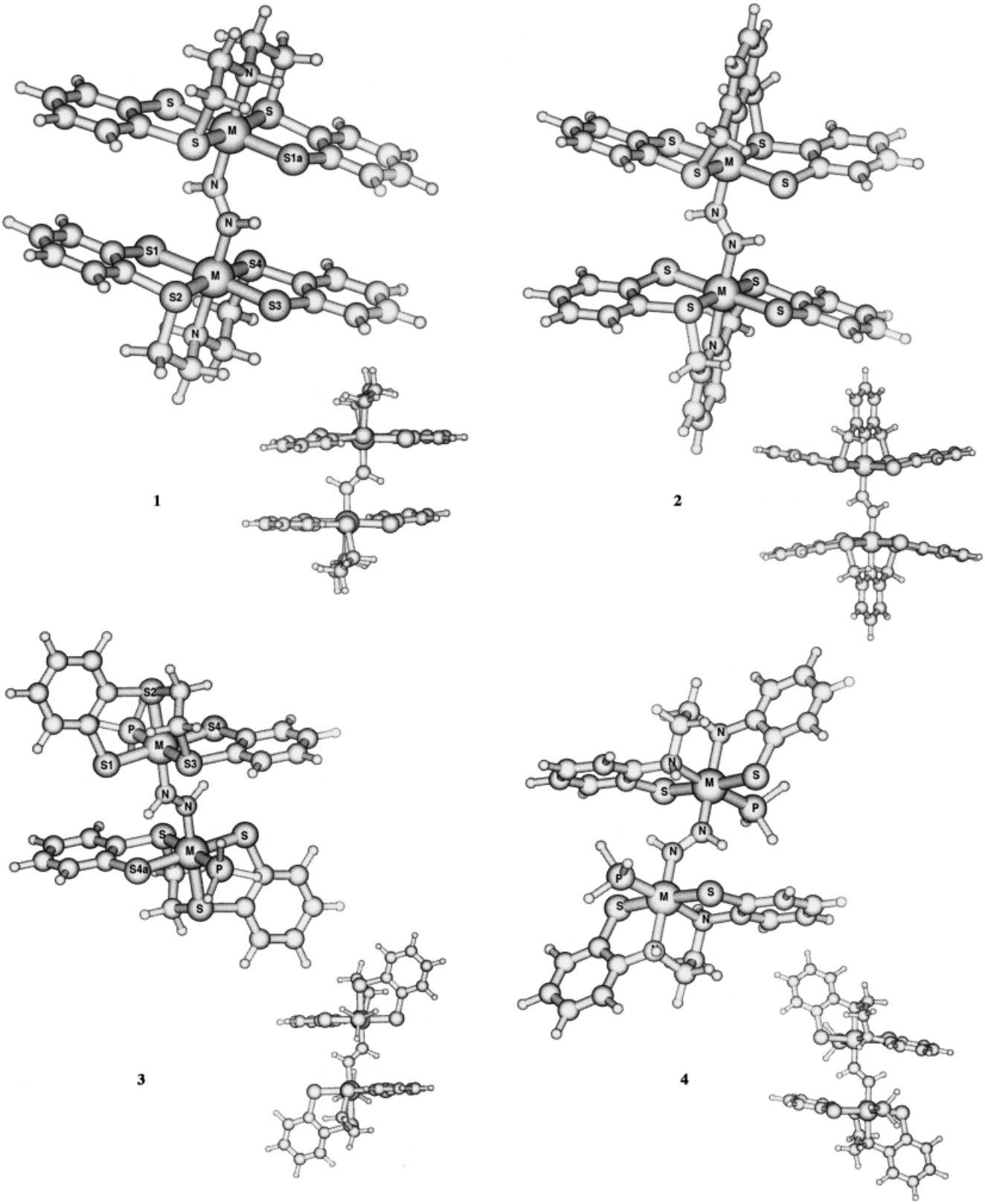

Figure 1. Optimized structure of complexes **1**–**4**. C_i point group symmetry, M = Fe, Ru, optimum view (large), side view (small).

While the dependence of the hydrogen bond energies on the density functional is negligible for type **1** and **2** complexes, it is larger in the case of **3** and **4**. Since B3LYP energetic data are considered to be generally more reliable for molecules consisting of main group atoms, we always recommend the B3LYP/TZVP data as the best data obtained—bearing in mind that the hydrogen bonds connect atoms that are second- and third-row elements. The comparison with the small basis set and with the nonhybrid BP86 functional serves as a test on internal consistency: we aimed at energetic data that are

0947-6539/01/0723-5198 $ 17.50+.50/0 *Chem. Eur. J.* **2001**, *7*, No. 23

Table 1. Comparison of selected bond lengths d [pm] and angles α [°] obtained from DFT calculations and X-ray diffraction experiments for the Fe^{II}–**1** complex.[a]

	BP86/RI	B3LYP	exp. [18]
d_{FeS1}[b]	233.0	237.4	231.8
d_{FeS2}	225.7	231.9	223.4
d_{FeS3}	231.8	236.1	228.8
d_{FeS4}	225.4	232.0	225.1
$d_{FeN(amine)}$	207.6	210.0	203.7
$d_{FeN(diaz)}$	188.2	193.5	186.7
d_{NN}	128.6	125.4	130.0
$d_{N(diaz)H}$	104.0	103.2	116.2
d_{S3H}	271.8	276.0	278.0
d_{S1aH}	245.7	249.1	220.1
$\alpha_{FeN(diaz)N(diaz)}$	132.5	133.1	132.2
$\alpha_{FeN(diaz)H}$	118.1	117.2	124.7
$\alpha_{N(diaz)N(diaz)H}$	109.4	109.7	103.1
$\alpha_{N(amine)FeN(diaz)}$	179.4	179.4	179.5
$\alpha_{S1FeN(diaz)}$	92.8	92.1	91.5
$\alpha_{S2FeN(diaz)}$	93.8	94.5	93.1
$\alpha_{S3FeN(diaz)}$	88.7	88.5	87.7
$\alpha_{S4FeN(diaz)}$	93.1	93.7	93.4

[a] The DFT results were obtained with the TZVP basis set. [b] The numbering of the sulfur atoms is given in Figure 1.

Table 2. Comparison of selected bond lengths d [pm] and angles α [°] obtained from DFT calculations and X-ray diffraction experiments for the Fe^{II}–**3** complex.[a]

	BP86/RI	B3LYP	exp. [20]	
			PPr_3	PEt_3
d_{FeS1}[b]	232.6	236.1	231.0	230.3
d_{FeS2}	227.5	233.7	225.7	222.6
d_{FeS3}	227.6	233.1	229.2	226.3
d_{FeS4}	231.5	235.3	230.8	229.9
d_{FeP}	222.0	229.0	226.3	226.6
d_{FeN}	189.5	193.7	190.0	187.5
d_{NN}	128.4	125.3	128.8	134.9
d_{NH}	104.4	103.7	106.1	92.1
d_{S1H}	279.9	284.0	281.4	284.6
d_{S4aH}	240.1	238.9	235.8	248.5
α_{FeNN}	130.7	131.3	131.7	132.4
α_{FeNH}	121.1	120.4	123.3	123.7
α_{S3FeP}	179.6	178.0	179.1	177.1
α_{NFeP}	90.8	90.8	88.1	88.8
α_{NFeS2}	178.2	177.6	176.8	175.3
α_{S1FeS4}	178.0	178.3	175.0	170.5
α_{NFeS1}	88.9	89.3	88.3	89.6
α_{S1FeS2}	89.3	88.3	88.5	87.7
α_{S1FeS3}	88.9	90.4	87.1	83.9

[a] Note that experimentally PPr_3 and PEt_3 ligands have been used for Fe^{II}-**3**, while in the DFT calculations PH_3 has been employed. The DFT results were obtained with the TZVP basis set. [b] The numbering of the sulfur atoms is given in Figure 1.

internally consistent regardless of whether a double-zeta or triple-zeta basis set was chosen and which functional was used.

The strongest *short* hydrogen bonds were found in complex **3** and amounted to 20–25 kJ mol^{-1} (depending on the functional) for Fe^{II}, to 15–21 kJ mol^{-1} for Fe^{III}, and to 20–21 kJ mol^{-1} for Ru^{II}. All other short hydrogen bonds were, in general, of similar strength, that is, about

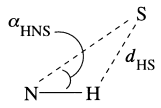

Figure 2. Definition of distance d_{HS} and α_{HNS}.

Table 3. Structural characteristics of the NH···S hydrogen bridges in iron complexes: lengths d_{HS} are given in pm and angles α_{HNS} in degrees. The case of a linear hydrogen bridge corresponds to $\alpha_{HNS} = 0$.

metal	complex	BP86/RI				B3LYP			
		SV(P)		TZVP		SV(P)		TZVP	
		d_{HS}	α_{HNS}	d_{HS}	α_{HNS}	d_{HS}	α_{HNS}	d_{HS}	α_{HNS}
Fe^{II}	**1**	244	37.9	246	37.6	246	36.7	249	36.9
		270	66.9	272	66.9	274	65.9	276	66.0
Fe^{III}	**1**	244	39.7	246	39.2	252	41.8	253	41.3
		272	68.4	273	68.3	278	69.7	280	69.6
Fe^{II}	**2**	237	36.5	240	36.1	242	35.9	244	35.6
		266	64.9	268	65.7	273	65.3	275	65.9
Fe^{III}	**2**	247	39.1	248	38.8	257	42.4	255	40.7
		271	67.1	272	67.2	280	69.9	281	69.4
Fe^{II}	**3**	237	35.3	240	35.9	238	33.9	239	33.5
		276	69.6	280	70.3	282	68.8	284	69.3
Fe^{III}	**3**	248	39.2	248	38.5	247	38.1	246	36.6
		274	70.8	277	71.2	277	70.1	278	70.1
Fe^{II}	**4**	254	40.8	255	40.8	240	34.1	242	34.2
		283	71.0	286	71.8	286	69.0	289	69.5
Fe^{III}	**4**	266	46.0	265	44.9	267	45.1	261	41.9
		277	71.9	279	72.2	280	71.2	281	70.7

Table 4. Structural characteristics of the NH···S hydrogen bridges in ruthenium complexes: lengths d_{HS} are given in pm and angles α_{HNS} in degrees. The case of a linear hydrogen bridge corresponds to $\alpha_{HNS} = 0$.

metal	complex	BP86/RI				B3LYP			
		SV(P)		TZVP		SV(P)		TZVP	
		d_{HS}	α_{HNS}	d_{HS}	α_{HNS}	d_{HS}	α_{HNS}	d_{HS}	α_{HNS}
Ru^{II}	**1**	250	35.2	254	35.6	254	35.4	257	35.7
		287	68.3	287	68.1	288	67.4	288	67.2
Ru^{II}	**2**	244	34.4	248	35.1	248	34.5	253	35.0
		284	67.2	284	67.3	287	66.9	287	66.7
Ru^{II}	**3**	234	31.2	238	31.5	240	32.1	244	32.4
		301	72.0	301	71.8	302	71.0	303	70.9
Ru^{II}	**4**	271	45.0	272	43.9	253	36.2	257	36.8
		319	78.8	320	78.8	311	73.2	314	74.1

Table 5. Shared-electron numbers and resulting hydrogen bond energies $E^{SEN}_{(HS)_i}$ in kJ mol^{-1} for compounds **1**–**4** with M = Fe^{II} and their oxidized dicationic analogues with M = Fe^{III}. Only two entries are given because of C_i symmetry. The short hydrogen bonds are given first. No shared-electron number is given if it drops below the threshold of $\sigma_{HS} = 0.005$.

metal	complex	BP86/RI				B3LYP			
		SV(P)		TZVP		SV(P)		TZVP	
		σ_{HS}	$E^{SEN}_{(HS)_i}$	σ_{HS}	$E^{SEN}_{(HS)_i}$	σ_{HS}	$E^{SEN}_{(HS)_i}$	σ_{HS}	$E^{SEN}_{(HS)_i}$
Fe^{II}	**1**	0.0360	18	0.0403	15	0.0324	21	0.0337	17
		0.0103	5.1	0.0129	4.9	0.0090	5.7	0.0110	5.7
Fe^{III}	**1**	0.0289	14	0.0328	13	0.0220	14	0.0251	13
		–	–	0.0052	2.0	–	–	–	–
Fe^{II}	**2**	0.0465	23	0.0506	19	0.0374	24	0.0401	21
		0.0129	6.4	0.0149	5.7	0.0101	6.4	0.0112	5.8
Fe^{III}	**2**	0.0270	13	0.0308	12	0.0187	12	0.0236	12
		0.0050	2.5	0.0060	2.3	–	–	–	–
Fe^{II}	**3**	0.0513	25	0.0514	20	0.0449	29	0.0489	25
		0.0050	2.5	0.0051	2.0	–	–	–	–
Fe^{III}	**3**	0.0344	17	0.0405	15	0.0340	22	0.0405	21
		0.0051	2.5	0.0053	2.0	–	–	–	–
Fe^{II}	**4**	0.0232	12	0.0297	11	0.0395	25	0.0430	22
		–	–	–	–	–	–	–	–
Fe^{III}	**4**	0.0122	6.0	0.0192	7.3	0.0113	7.2	0.0210	11
		–	–	0.0056	2.1	–	–	–	–

Table 6. Shared-electron numbers and resulting hydrogen bond energies $E^{SEN}_{(HS)_i}$ for compounds **1**–**4** with M = Ru. Note that only two entries are given because of C_i symmetry. The short hydrogen bonds are given first. No shared electron number is given if it drops below the threshold of $\sigma_{HS} = 0.005$.

metal	complex	BP86/RI				B3LYP			
		SV(P)		TZVP		SV(P)		TZVP	
		σ_{HS}	E^{SEN}_{HS}	σ_{HS}	E^{SEN}_{HS}	σ_{HS}	E^{SEN}_{HS}	σ_{HS}	E^{SEN}_{HS}
Ru^{II}	**1**	0.0291	14	0.0313	12	0.0238	15	0.0255	13
		0.0057	2.8	0.0083	3.2	0.0053	3.4	0.0073	3.8
Ru^{II}	**2**	0.0377	19	0.0387	15	0.0296	19	0.0303	16
		0.0066	3.3	0.0088	3.3	0.0056	3.6	0.0074	3.8
Ru^{II}	**3**	0.0508	25	0.0527	20	0.0386	25	0.0411	21
		–	–	–	–	–	–	–	–
Ru^{II}	**4**	0.0103	5.1	0.0156	5.9	0.0214	14	0.0253	13
		–	–	–	–	–	–	–	–

13 kJ mol^{-1} for Fe^{III} and Ru^{II} and about 20 kJ mol^{-1} for Fe^{II}.

For Fe^{III} we found smaller hydrogen bond energies compared with the Fe^{II} analogues. The hydrogen bonds in the Ru^{II} complexes are also, in general, weaker than those in their Fe^{II} analogues. The difference in hydrogen bond energies can be understood in view of different H···S lengths. The hydrogen bond energy decreases almost linearly with increased distance by about −4 kJ per mol per 10 pm (the correlation coefficient for this linear relationship is for all functionals and basis sets larger than 0.94). This linear dependence is remarkable since the hydrogen bridges are not linear but show a strong angular variation; the variety of different angles is given in Tables 3 and 4.

We are well aware that the calculation of hydrogen bond lengths by means of DFT can be problematic because DFT cannot describe dispersion interactions, which may contribute of the order of ⅓ of the hydrogen bond interaction (for a discussion of the reliability of DFT for hydrogen bonds, see Part I and Refs. [29–31]). In the case at hand, however, we came to valid conclusions despite of this shortcoming of DFT, because the rigid molecular structure enforces a H···S length that is determined by the N–H, N–N, N–Fe, and Fe–S lengths and corresponding angles. The H···S length thus depends on the accurately reproduced Fe–S bond length rather than on the insufficiently described dispersion interaction in H···S. Consequently, the potential well for the hydrogen bond interaction is dominated by the covalent N–H bond energy and is not shallow but rather deep.

Since all complexes under study are very similar, the error in the calculated hydrogen bond lengths is systematic and the values for the hydrogen bond lengths may be used in the design of nitrogenase model complexes as a qualitative and experimentally easily accessible measure for the hydrogen bond energy.

Total hydrogen bond energies: To determine the total hydrogen bond energy, E^{SEN}_{HS}, for every dinuclear complex, we summed all its individual hydrogen bond energies:

$$E^{SEN}_{HS} = \sum_i E^{SEN}_{(HS)_i} \quad (2)$$

The results are given in Table 7. With respect to the accuracy of total hydrogen bond energies, we note that the error in single $E^{SEN}_{(HS)_i}$ energies is more severe owing to C_1 symmetry, because for the four hydrogen bridges it is exactly twice the error of the two individual hydrogen bonds.

Table 7. Total hydrogen bond energies $E^{SEN}_{HS} = \sum_i E^{SEN}_{(HS)_i}$ in kJ mol^{-1} estimated from shared-electron numbers as the sum of the values given in Tables 5 and 6.

metal	complex	BP86/RI		B3LYP	
		SV(P)	TZVP	SV(P)	TZVP
Fe^{II}	**1**	46	40	53	46
	2	59	50	61	53
	3	56	43	57	50
	4	23	23	51	44
Fe^{III}	**1**	29	29	28	26
	2	32	28	24	24
	3	39	35	43	42
	4	12	19	14	22
Ru^{II}	**1**	34	30	37	34
	2	44	36	45	39
	3	50	40	49	42
	4	10	12	27	26

Furthermore, in all cases in which the energy of the long hydrogen bond drops below the SEN threshold of $\sigma_{HS} = 0.005$, individual hydrogen bonds with energies of < 2 kJ mol^{-1} are not tracked at all, since these weak hydrogen bonds cannot be calculated reliably by our approach. This uncertainty affects the total hydrogen bond energies, for which the potential contribution of two very weak hydrogen bonds might amount to < 4 kJ mol^{-1}. It explains the difference in total hydrogen bond energies obtained with the two density functionals for Fe^{III}–**2**, with BP86/RI the two weak (long) hydrogen bonds were detected, while they are below the threshold with B3LYP. However, in general, the effect is negligible as can be seen from the other cases.

From the B3LYP/TZVP results it can be seen that the total hydrogen bond energies E^{SEN}_{HS} range from about 22 to 53 kJ mol^{-1}. As one would expect from the discussion of single hydrogen bridges, the Fe^{II} complexes exhibit the largest total hydrogen bond energies.

Since every hydrogen atom of *trans*-diazene belongs to a short and to a long hydrogen bridge simultaneously, such that a bifurcated structure can develop, the question arises as to whether the total energy of this bifurcated structure can be calculated by adding the energies of a short and long hydrogen bond. To answer this question we compared the B3LYP/TZVP data for the dinuclear Fe^{II} complex **1** with data obtained for its mononuclear analogue in Part I, which is 29 kJ mol^{-1} for one short plus one long hydrogen bond. We found that for **1** the total hydrogen bond energy (46 kJ mol^{-1}) is 12 kJ mol^{-1} smaller than the doubled value found for the mononuclear analogue (2×29 kJ mol^{-1}); this indicates that the strength of the individual hydrogen bonds is considerably decreased in the bifurcated structure.

Contribution of hydrogen bonding to the total stabilization of diazene: In order to calculate the contribution of hydrogen bonding to the total stabilization energy, ΔE_{stab}, of the diazene

0947-6539/01/0723-5200 $ 17.50+.50/0 *Chem. Eur. J.* **2001**, *7*, No. 23

moiety in dinuclear diazene complexes, the stabilization energies can be evaluated according to the reaction:

$$N_2H_2 + 2[M] \rightarrow [M]\text{-NH-HN-}[M] \qquad \Delta E_{stab} \qquad (3)$$

in which [M] symbolizes the five-coordinate metal fragment. Since all model complexes contain at least two strong H···S hydrogen bridges (NB an ordinary H···S bond is usually not stronger than about 5 kJ mol^{-1}), their total contribution to the diazene stabilization energy ΔE_{stab} can become fairly large. All molecules in reaction (3) possess singlet ground states if M = Ru^{II}. This, however, is not the case for M = Fe^{II} because the five-coordinate metal fragments [Fe^{II}] possess ground states of higher multiplicity. The case M = Fe^{III} is not considered here since doublet and quartet multiplicities must also be taken into account, which is out of reach of current density functional calculations as will become obvious in the following analysis of the Fe^{II} reaction energetics.

The five-coordinate fragments [Fe^{II}] are predicted to have triplet or singlet ground states in BP86/RI calculations, while B3LYP yields quintet ground states. Table 8 gives values for ΔE_{stab} obtained with BP86/RI and B3LYP for Fe^{II} and Ru^{II} complexes in their ground states, as predicted by the particular density functionals. While the absolute values of the Ru^{II} reaction energies are larger for BP86/RI by up to about 40 kJ mol^{-1} when compared with B3LYP, this difference is increased for Fe^{II} complexes to about 180 kJ mol^{-1}. Additionally, the absolute values are larger for the Ru^{II} cases than for Fe^{II}. Consequently, with some care it is possible to draw conclusions from the calculated reaction energies for Reaction (3) if M = Ru^{II}, while it is hardly possible to interpret the Fe^{II} energetic data at all. The ΔE_{stab} values have not yet been corrected for the basis set superposition error, since the results obtained with different functionals vary such that is not yet worthwhile to calculate a counter-poise correction.

Table 8. Stabilization energies ΔE_{stab} in kJ mol^{-1} at 0 K obtained according to Reaction (3) with the TZVP basis set for Fe^{II} and Ru^{II} complexes (without zero-point vibrational energy corrections). Our results show that BP86/RI and B3LYP calculations cannot be used to determine the ΔE_{stab} for Fe^{II} complexes reliably (cf. the discussion in the text).[a]

metal	complex	BP86/RI		B3LYP	
		ΔE_{stab}	M	ΔE_{stab}	M
Fe^{II}	**1**	−227 (18%)	T	−65.5 (70%)	Q
	2	−261 (19%)	S	−82.3 (64%)	Q
	3	−254 (17%)	T	−87.5 (57%)	Q
	4	−268 (9%)	T	−89.6 (49%)	Q
Ru^{II}	**1**	−343 (9%)	S	−298 (11%)	S
	2	−310 (12%)	S	−280 (14%)	S
	3	−274 (15%)	S	−254 (17%)	S
	4	−324 (4%)	S	−283 (9%)	S

[a] All dinuclear complexes are calculated as singlet states. The ground state multiplicities obtained for the five-coordinate metal fragments [M] are given in column M (S = singlet, T = triplet, Q = quintet). The contribution of the total hydrogen bond energies from Table 7 to diazene stabilization as a percentage of the stabilization energy ΔE_{stab} is given in parentheses.

The investigation of the energetics of Reaction (3) clearly demonstrates that current density functional calculations cannot reliably predict differences in total energies for iron compounds in which spin states of different multiplicity are energetically close. As a consequence, reliable stabilization energies ΔE_{stab} cannot be obtained for Fe^{II} complexes. This result is in accordance with observations made by comparison of calculated ground-state multiplicities with experimentally found magnetic properties of fully characterized complexes such as [Fe(L)('NHS$_4$')] with L = N_2H_4, NH_3, CO, NO^+, PR_3.[32]

In spite of these results, we may extract lower and upper boundaries for the contribution of the hydrogen bonding interactions to the total stabilization energy ΔE_{stab}; for this analysis we rely on the fact that the errors in results from both functionals are *systematic* (cf. Ref. [32]). The BP86/RI/TZVP calculations favoring singlet or triplet ground states for the metal complex fragments [Fe^{II}] yield a lower boundary for the hydrogen bond energy contribution to ΔE_{stab} in Fe^{II} complexes. As Table 8 demonstrates, we obtain a contribution by hydrogen bonds to the stabilization energy ΔE_{stab} in Fe^{II} complexes of about 20%. B3LYP calculations, on the other hand, favor high-spin multiplicities such that B3LYP stabilizes the high-spin quintet states of the five-coordinate [Fe^{II}] metal fragments too much. This overemphasis of the quintet state stability of [Fe^{II}] fragment molecules results in a reduced reaction energy ΔE_{stab} for Reaction (3), which is the difference of the total electronic energies for the dinuclear product molecule and for the two [Fe^{II}] complex fragments plus diazene. The ΔE_{stab} values from B3LYP calculations are therefore too small, and the hydrogen bonding contribution to diazene stabilization comes out too large. We thus come to the conclusion that the BP86/RI and B3LYP data in Table 8 yield lower and upper boundaries, respectively, for the hydrogen bond energy contribution to ΔE_{stab}.

For Ru^{II} we arrive at a hydrogen bonding contribution to diazene stabilization of only about 10%, which is due to the strong Ru–N bonds in the dinuclear complex resulting in large binding energies.

Conclusion

Our analysis of nitrogenase model complexes containing ligands with biologically compatible donor-atom sets and metal centers leads us to the following conclusions. Bifurcated hydrogen bridges are only found in dinuclear complexes **1** and **2** with Fe^{II} centers. All other complexes contain only two nonbifurcated hydrogen–sulfur bonds. For **1** with Fe^{II}, a total hydrogen bond energy of 70 kJ mol^{-1} has been estimated.[18] The result is in fair agreement with the SEN value E_{HS}^{SEN} of 46 kJ mol^{-1} for the total hydrogen bond energy in Fe^{II}–**1**.

The compounds with Fe^{II} centers exhibit stronger hydrogen bonds than their Fe^{III} analogues. This is an important observation with respect to the mechanism proposed in Scheme 3. The protonation of the ligand-sphere thiolate donors in Scheme 3A yields the dicationic species B. A consecutive intramolecular proton and electron transfer onto molecular nitrogen bridging the two metal centers yields

intermediate C. The reduction of structure C to D would then stabilize the diazene thus created through an increase in hydrogen bond strength.

While the hydrogen bonds could stabilize dinuclear Fe^{II} complexes by more than 20%, this effect is strongly reduced for Ru^{II} compounds, in which the binding energy of diazene to Ru^{II} itself is comparatively large. Ru^{II} stabilizes the diazene ligand mainly through this large binding energy. The hydrogen bond energies are smaller than those in the analogous Fe^{II} complexes and do not play a significant role in the stabilization of N_2H_2. The increased stabilization of unstable N_2H_2 by Ru complexes is thus mainly due to the greater strength of the Ru–N bonds in the Ru-N_2H_2-Ru entity.

Fine tuning of the hydrogen bond energy can be achieved through changing the hydrogen–sulfur bond lengths. The H···S lengths vary when different chelate ligands (penta- vs. tetradentate) coordinate the metals, when iron is replaced by ruthenium to yield complex fragments with different metal–sulfur lengths, or when the formal oxidation states and/or the spin states of the metal centers change.

In the light of such large contributions of hydrogen bonding to the stabilization of N_2H_x species, the role of hydrogen bonding can hardly be overestimated during a reduction from molecular nitrogen to ammonia.

Computational Methods

For all calculations we used the density functional programs provided by the TURBOMOLE 5.1 suite.[33] We employed the Becke–Perdew functional dubbed BP86[34, 35] and the hybrid functional B3LYP[36, 37] as implemented in TURBOMOLE. Moreover, we always used the resolution of the identity (RI) technique for the BP86 functional.[38, 39] For all compounds containing ruthenium we employed the effective core potentials from the Stuttgart group[40] as implemented in TURBOMOLE. All results were obtained from all-electron Kohn–Sham calculations.

The influence of the size of the basis set was studied by means of two different basis sets, the first denoted SV(P). This is the Ahlrichs split-valence basis set with polarization functions on heavy atoms, but not on hydrogen atoms.[41] Moreover, the TZVP basis featuring a valence triple-zeta basis set with polarization functions on all atoms was used.[42] All structures were optimized with the corresponding basis set. In order to analyze the electron density of the compounds, we made use of the concept of shared-electron numbers as implemented in TURBOMOLE. Details of the SEN method are described in Part I.[27]

The program Molden was used for the visualization of structures.[43]

[1] M. Reiher, D. Sellmann, B. A. Hess, *Theor. Chem. Acc.* **2001**, *106*, 379–392.
[2] B. K. Burgess, D. J. Lowe, *Chem. Rev.* **1996**, *96*, 2983–3012.
[3] R. R. Eady, *Chem. Rev.* **1996**, *96*, 3013–3030.
[4] J. B. Howard, D. C. Rees, *Chem. Rev.* **1996**, *96*, 2965–2982.
[5] M. Hidai, Y. Mizobe, *Chem. Rev.* **1995**, *95*, 1115–1133.
[6] R. A. Henderson, G. J. Leigh, C. J. Pickett, *Adv. Inorg. Chem. Radiochem.* **1983**, *27*, 198–292.
[7] Y. Nishibayashi, I. Wakiji, K. Hirata, M. Rakowski du Bois, M. Hidai, *Inorg. Chem.* **2001**, *40*, 578–580.
[8] Y. Nishibayashi, S. Iwai, M. Hidai, *Science* **1998** *279*, 540–542.
[9] C. J. Pickett, *J. Biol. Inorg. Chem.* **1996**, *1*, 601–606.
[10] G. J. Leigh, *Eur. J. Biochem.* **1995**, *229*, 14–20.
[11] E. I. Stiefel in *Recent Developments in Nitrogen Fixation* (Eds.: W. Newton, J. R. Postgate, C. Rodriguez-Barrueco), Academic Press, London, **1977**, pp. 69–108.
[12] G. H. Aylward, T. J. V. Findlay, *Datensammlung Chemie*, Verlag Chemie, Weinheim, **1975**.
[13] *Lexikon der Biochemie und Molekularbiologie*, Herder, Freiburg, **1992**, p. 179.
[14] D. Sellmann, J. Sutter, *J. Biol. Inorg. Chem.* **1996**, *1*, 587–593.
[15] D. Sellmann, J. Sutter, *Acc. Chem. Res.* **1997**, *30*, 460–469.
[16] D. Sellmann, A. Fürsattel, *Angew. Chem.* **1999**, *111*, 2142–2145; *Angew. Chem. Int. Ed.* **1999**, *38*, 2023–2026.
[17] R. W. F. Hardy in *A Treatise on Dinitrogen Fixation* (Eds.: R. W. F. Hardy, F. Bottomley, R. C. Burns), Wiley, New York, **1979**, Chapter 4, pp. 515–568.
[18] D. Sellmann, W. Soglowek, F. Knoch, M. Moll, *Angew. Chem.* **1989**, *101*, 1244–1245; *Angew. Chem. Int. Ed.* **1989**, *28*, 1271–1272.
[19] D. Sellmann, W. Soglowek, F. Knoch, G. Ritter, J. Dengler, *Inorg. Chem.* **1992**, *31*, 3711–3717.
[20] D. Sellmann, H. Friedrich, F. Knoch, M. Moll, *Z. Naturforsch.* **1993**, *48b*, 76–88.
[21] D. Sellmann, A. Hennige, F. W. Heinemann, *Inorg. Chim. Acta* **1998**, *280*, 39–49.
[22] D. Sellmann, T. Becker, F. Knoch, *Chem. Eur. J.* **1996**, *2*, 1092–1098.
[23] G. E. Hoch, K. C. Schneider, R. H. Burris, *Biochim. Biophys. Acta* **1960**, *37*, 273–279.
[24] B. K. Burgess, S. Wherland, W. E. Newton, E. I. Stiefel, *Biochemistry* **1981**, *20*, 5140–5146.
[25] D. Sellmann, A. Fürsattel, J. Sutter, *Coord. Chem. Rev.* **2000**, *200–202*, 541–561.
[26] J. P. Collman, J. E. Hutchison, M. S. Ennis, M. A. Lopez, R. Guilard, *J. Am. Chem. Soc.* **1992**, *114*, 8074–8080.
[27] T. Gottschalk-Gaudig, PhD thesis, University of Erlangen-Nuremberg (Germany), **1997**.
[28] D. Sellmann, S. Emig, F. W. Heinemann, F. Knoch, *Z. Naturforsch.* **1998**, *53b*, 1461–1474.
[29] K. Kim, K. D. Jordan, *J. Phys. Chem.* **1994**, *98*, 10089–10094.
[30] J. J. Novoa, C. Sosa, *J. Phys. Chem.* **1995**, *99*, 15837–15845.
[31] M. Lozynski, D. Rusinska-Roszak, H.-G. Mack, *J. Phys. Chem. A* **1998**, *102*, 2899–2903.
[32] M. Reiher, O. Salomon, B. A. Hess, *Theor. Chem. Acc.* **2001**, in press.
[33] R. Ahlrichs, M. Bär, M. Häser, H. Horn, C. Kölmel, *Chem. Phys. Lett.* **1989**, *162*, 165–169.
[34] A. D. Becke, *Phys. Rev. A* **1988**, *38*, 3098–3100.
[35] J. P. Perdew, *Phys. Rev. B* **1986**, *33*, 8822–8824.
[36] A. D. Becke, *J. Chem. Phys.* **1993**, *98*, 5648–5652.
[37] P. J. Stephens, F. J. Devlin, C. F. Chabalowski, M. J. Frisch, *J. Phys. Chem.* **1994**, *98*, 11623–11627.
[38] K. Eichkorn, O. Treutler, H. Öhm, M. Häser, R. Ahlrichs, *Chem. Phys. Lett.* **1995**, *240*, 283–290.
[39] K. Eichkorn, F. Weigend, O. Treutler, R. Ahlrichs, *Theor. Chem. Acc.* **1997**, *97*, 119–124.
[40] D. Andrae, U. Häußermann, M. Dolg, H. Stoll, H. Preuß, *Theor. Chim. Acta* **1990**, *77*, 123–141.
[41] A. Schäfer, H. Horn, R. Ahlrichs, *J. Chem. Phys.* **1992**, *97*, 2571–2577.
[42] A. Schäfer, C. Huber, R. Ahlrichs, *J. Chem. Phys.* **1994**, *100*, 5829–5835.
[43] G. Schaftenaar, J. H. Noordik, *J. Comput.-Aided Mol. Des.* **2000**, *14*, 123–134.

Received: July 13, 2001 [F3414]

  0947-6539/01/0723-5202 $ 17.50+.50/0